International Journal of Environmental Science and Technology
https://doi.org/10.1007/s13762-023-04792-1

SHORT COMMUNICATION

# Synthesis of bimetallic FeMn nanoparticles using rooibos tea extract: characterization and application

**N. Böke[1] · K. F. Kapiamba[2] · E. Kimpiab[3] · H. O. Otor[4] · L. Petrik[1,3]**

Received: 3 August 2022 / Revised: 21 December 2022 / Accepted: 20 January 2023


## Abstract

Bimetallic FeMn nanoparticles based on a ferromanganese wad were successfully synthesized employing an entirely green approach. South African rooibos tea (RTea) extract was used as an environmentally friendly reducing and capping agent for preparing the Fe and Mn nanoparticles (nFeMn). The obtained nFeMn suspension and freeze-dried RTea capped nFeMn powder were characterized using several techniques. Elemental analysis conducted using XRF combined with ICP analysis revealed a metallic loading of 1.08 wt% of Fe and 0.25 wt% of Mn. The ultraviolet–visible spectroscopy (UV–vis) showed a broad shoulder in the UV region where the peaks of RTea and FeMn are located, implying bond formation during the reaction between RTea polyphenols and nFeMn. TEM analysis depicted a core–shell architecture for the nFeMn with an average size of 20 nm while the FTIR revealed that specific peaks observed in the spectrum of RTea extract were visible on that of the nFeMn powder, indicating the capping of nFeMn particles by the RTea extract. Finally, the reactivity of nFeMn powder as a Fenton-like reagent was probed for the decoloration of methylene blue (MB) from an aqueous solution. Fenton-like oxidation of MB followed a pseudo-first-order reaction kinetics with a rate constant of 0.23 $A^{-1}$ $min^{-1}$. The results showed that nFeMn removed MB dye with an efficiency of over 95% in the MB concentration range of 50–250 mg/L. Overall, the finding herein is unique because we directly used readily available raw material as a source of metals and a safe, practical reagent to prepare bimetallic FeMn nanoparticles that can be used to remove the color from dye wastewater, thus, creating a circular green process.

**Keywords** Ferromanganese wad · Bimetallic FeMn nanoparticles · Rooibos tea · Fenton-like oxidation

## Introduction

Research on bimetallic nanoparticles has been ongoing for the past thirty years, with interest generated by their exhibited enhanced activity in several reactions compared to their monometallic counterparts (Toshima and Yonezawa 1998; Doan et al. 2022; Sivashankar et al. 2022). The improved catalytic activity could be related to changes in electronic structure, geometric effects, and modification of the catalyst morphology (Yang and Somorjai 2004; Gilroy et al. 2016; Loza et al. 2020; Yoo et al. 2020). Bimetallic nanoparticles have been shown to have different topologies, such as crown-jewel structure, hollow structure, heterostructure, alloyed structure, and porous structure (Duan et al. 2020; Lin et al. 2022; Suliz et al. 2022; Zhang et al. 2022). In addition, some bimetallic materials exist in core–shell structures with a dense core and a thin shell, while alloyed nanoparticles with uniform textural properties have also been reported (Liu et al. 2012). Bimetallic nanoparticles can be prepared via

Editorial responsibility: Fatih ŞEN.

✉ K. F. Kapiamba
kapiamba.kashalafabrice@mst.edu

[1] Environmental and Nano Science Research Group, Department of Chemistry, University of the Western Cape, Cape Town 7535, South Africa

[2] Department of Civil, Architectural and Environmental Engineering, Missouri University of Science and Technology, Rolla, MO 65409, USA

[3] Department of Chemical Engineering, Cape Peninsula University of Technology, Symphony Way, PO Box 1906, Bellville, Cape Town 7535, South Africa

[4] Department of Chemical and Biomolecular Engineering, University of Notre Dame, South Bend, IN 46556, USA

Published online: 31 January 2023

solution chemistry using co-reduction, successive reduction, or reduction of double complexes. The first method relates to the simultaneous reduction of metal salts (Ahmed and Emam 2019). The second method is one of the most suitable methods for preparing core–shell bimetallic particles and comprises the reduction of one metal followed by that of the second metal. The third method involves co-reduction of the metals in a compound containing two metals, e.g., preparation of Ag-Pt bimetallic particles from silver(I) bis(oxalato)platinate(I) (Toshima and Yonezawa 1998; Liu et al. 2012; Bai et al. 2017; Deng et al. 2021). In solution, bimetallic nanoparticles may aggregate into larger particles without a stabilizer. Poly(N-vinyl-2-pyrrolidone) (PVP) is the most frequently used stabilizer to synthesize bimetallic nanoparticles with $NaBH_4$ as a reductant (Fang et al. 2011; Du et al. 2021; Ramos and Regulacio 2021; Tiri et al. 2022). Meanwhile, even when dissolved in small quantities, PVP and $NaBH_4$ produce hazardous compounds in the reaction environment.

Dried leaves or plant extracts may act as stabilizers and reductants in synthesizing bimetallic nanoparticles due to their polyphenolic compounds. Thus, they can be a viable alternative to traditional chemicals used for this purpose (Shankar et al. 2004; Kimpiab et al. 2022). For example, extracts of neem (*Azadirachta indica*), persimmon (*Diopyros kaki*), mahogany (*Swietenia mahogani* JACQ.), cashew (*Anacardium occidentale*), and Sago Pondweed (*Potamogeton pectinatus* L.) leaves were used in the synthesis of Au/Ag core–shell nanoparticles; Ce Bai Ye (*Cacumen Platycladi*) and green tea leaves were employed to obtain AuPd and FePd nanoparticles (Shankar et al. 2004; Mondal et al. 2011; Sheny et al. 2011; Smuleac et al. 2011; Zhan et al. 2011).

In this work, the co-reduction method was used to synthesize ferromanganese wad-based FeMn nanoparticles utilizing the rooibos tea (RTea) extract as a reducing and capping agent. Rooibos (*Aspalathus linearis*) is indigenous to South Africa and growing in the Cederberg region. Ores (ferromanganese) containing high levels of Fe and Mn are abundant worldwide. Hence, these ores are often used as valuable nanoparticle synthesis resources (Chen et al. 2020; Zhang et al. 2020). In addition, Rooibos tea is a rich source of polyphenols; it is caffeine-free and possesses antioxidant properties (Iswaldi et al. 2011). The Folin–Ciocalteu assay (Paquin et al. 2015) determined the total polyphenolic content to be 25% (w/w) of an aqueous fermented rooibos tea extract of 10 g/L, indicating its potential to be a suitable reductant for metal nanoparticles. Aspalathin is the main flavonoid and antioxidant in rooibos (Baranska et al. 2006). Green synthesized bimetallic nanoparticles are desirable because, like their monometallic counterparts, they can be employed in environmentally friendly applications. Specifically, several studies show the use of monometallic, green-synthesized iron nanoparticles in removing organic or inorganic contaminants from aqueous solutions (Jin et al. 2018; Nasrollahzadeh et al. 2021; Ghohestani et al. 2022). But information on bimetallic green synthesized nanoparticles and their application to environmental remediation are limited.

The textile, leather, paper, and plastics industries are known to produce large volumes of colored wastewater. Two percent of dyes produced are directly released as aqueous effluent, and in the textile industry, 10% of the dyes are lost during the coloration process (Rai et al. 2005; Fatima et al. 2017). If not adequately treated, the effluent dyes contaminate soil and water sources. Monometallic nanoiron particles have previously been used for the remediation of dyes and found to effectively remove dyes by adsorption or decolorize them by Fenton-like oxidation processes (Mukherjee et al. 2016; Stefaniuk et al. 2016; Fazlzadeh et al. 2017; Badmus et al. 2018; Kimpiab et al. 2022).

A classical nano zerovalent iron (nZVI) synthesis comprises adding a chemical reductant, usually sodium borohydride, into an iron suspension of 0.1 M $Fe^{3+}$ without any dispersant. In this study, a different approach was followed in terms of using a FeMn acidic solution prepared from a mined ferromanganese wad as a source of metal precursors and adding polyphenols from an aqueous extract of a natural organic matter (RTea) as reductant and capping agent. The current study demonstrates the capability of the RTea-capped nFeMn particles as a Fenton-like catalyst to degrade azo dye methylene blue in an aqueous solution.

## Materials and methods

### Materials

The ferromanganese wad was obtained from Ryedale open-pit mine in the Ventersdorp district of South Africa. The FeMn wad was dried overnight at 90 ℃ and sieved to obtain a fraction below 0.5 µm, which was then stored in a closed container to synthesize nFeMn. The rooibos tea (RTea), in the form of leaves was fermented. All the chemicals used during several synthesis stages and Fenton-like reactions (HCl, NaOH, $H_2O_2$, methylene blue) were of analytical grades.

### Synthesis procedure

The aqueous RTea extract (20 g/L) was freshly prepared by heating the RTea/water mixture at 80 °C for 20 min, then filtering the leaves from the tea, followed by centrifugation of the filtrate. The reason for applying centrifugation, but not fine filtration, was that the tea extract plugged the filter paper's pores (both 0.22 and 0.45 µm) during vacuum filtration.

A mixture of natural ferromanganese wad mineral containing FeMn (2 g) and 200 mL of HCl (50% v/v) was heated at 90 °C for 10 min to dissolve the FeMn wad. Next, the obtained FeMn acidic solution was vacuum filtered through 0.45 µm filter paper and stored in a glass bottle. Next, 50 mL of filtered acidic FeMn solution was adjusted to pH = 1.70 because the extremely acidic solution (pH = 0) would destroy polyphenolic compounds in the RTea. After preparation, the pH-adjusted FeMn acidic solution was immediately added to the RTea extract with a volume ratio of 2:1; the volume ratio is based on the FeMn acidic solution, not on the pH-adjusted FeMn acidic solution (Hoag et al. 2009). The nFeMn suspension's color instantly turned black, and the suspension was kept in the dark for 24 h to complete the reaction. Afterward, the nFeMn suspension was poured into 40-mL plastic containers and freeze-dried for 6 days at − 53 °C. Finally, the obtained dried RTea- capped nFeMn powder was placed into a sealed container and stored in the dark in a desiccator to prevent oxidation of the metals.

### Characterization

The LOI (Loss on Ignition) was determined on a portion of the finely ground FeMn wad sample by heating in a muffle furnace to 950 °C using 0.65 g of the sample, which was accurately weighed with 5.6 g of Lithium Borate Flux (Claisse cat. # G-0640-70) and fused at 950 °C using a Claisse Fluxy M4 fuser and cast into a disk. The fusion disk was measured on a Panalytical PW2400 WDXRF fitted with a 3 kV rhodium tube. A range of 12 CRM's (Certified Reference Material) were used to calibrate the instrument for the elements determined using various combinations of collimators, crystals, and detection counters. To ensure the best resolution, a Spectro Arcos Inductively Coupled Plasma-Optical Electron Spectroscopy (ICP-OES) was used to analyze liquid samples. The instrument is equipped with Charge-Couple Device (CCD) detectors, and the radial view limits the matrix effects.

Ultraviolet–visible spectroscopy (UV–Vis) scanning of the solutions was done in the 200–800 nm range using Nicolette—Evolution 100 Ultraviolet Spectrophotometer (Thermal Electron Corporation, UK). Decolouration of MB was followed by reading the absorbance of standards prepared from an MB solution at 665 nm using a Portable Thermo Scientific Helios Epsilon UV/VIS spectrometer; sample concentrations were read off the calibration curve drawn up using the standards. Transmission electron microscopy (TEM) and Energy dispersive spectroscopy (EDS) measurements were done using a G2 F20 X Twin Mat 200 kV Tecnai FEG-TEM transmission electron microscope with EDS attachment. The X-ray diffraction (XRD) patterns of the FeMn wad and the powder samples were recorded on a Bruker powder diffractometer (D8 Advance) equipped with a theta-theta goniometer setting which includes a Cu target X-ray tube (CuKa1 line at k = 1.5406 Å) and PSD Vantec-1 detector. Data evaluation was done using the EVA software from Bruker based on the International Centre for Diffraction Data (ICDD) PDF database 1998.

### Decoloration experiments

Decoloration experiments were performed in an Erlenmeyer flask placed in a water bath at 25 °C. UV–vis absorbance of the reaction solutions was measured at 665 nm, where the MB solution gives maximum absorbance. 20 mg of nFeMn was added into 2 mL of 0.1% $H_2O_2$ and 18 mL of 50 mg/L MB solution. The Erlenmeyer containing the reaction mixtures was shaken in the water bath and was removed from the bath at specified times. The nFeMn particles were recovered by decantation from the reaction mixture, and absorbance values were recorded (Shahwan et al. 2011). In addition, the effect of MB concentration on the extent of decoloration was assessed by varying MB solutions' concentrations from 50 to 250 mg/L. Finally, the reaction mixtures prepared in the same manner above were shaken for an hour, filtered, and their UV–vis absorbance values were measured. Figure 1 is a schematic representation of the experimental approach.

## Results and discussion

### Characterization of synthesized nFeMn

A naturally occurring ferromanganese wad containing mainly $Fe_2O_3$ and MnO (57.5 and 15.2%, w, respectively) (Table 1A) was leached using HCl (50%, v/v) (see experimental section). After filtering, the FeMn acidic solution with mainly $Fe^{3+}$ and $Mn^{2+}$ (0.34 and 0.08%, w, respectively) (or $Fe^{3+}$ 0.61 M) (Table 1B) was obtained. The recovery resulting from the dissolution process of the FeMn wad was calculated to be 84.6% and 68.4% for Fe and Mn, respectively. This result indicates the loss of Fe and Mn together with the residue (mainly Si) during filtration of the FeMn acidic solution. The pH of the filtered FeMn acidic solution (50 mL) from the stock was adjusted (pH = 1.7) and added to RTea extract (20 g/L, w/v). Depending on the composition (Table 1A) and the amount of FeMn wad that was dissolved in the HCl (50%, v/v), the Fe and Mn concentrations in the FeMn acidic solution (Table 1B) and the amount of product made, it was possible to calculate the iron and manganese content of nFeMn powder (Table 1C). The reason for this is that the reaction mixture composed of pH-adjusted FeMn acidic solution and RTea extract was directly freeze-dried after mixing and aging for 24 h. That is, no filtration or centrifugation procedure leading to Fe loss was applied after the reaction, before the freeze-drying.

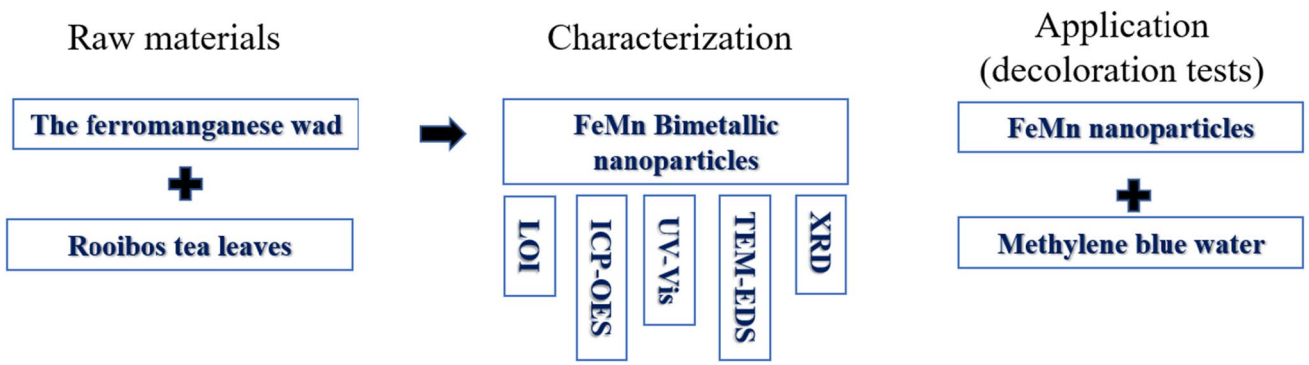


**Fig. 1** Brief schematic representation of synthesis process and catalytic assessment

The RTea-capped nFeMn powder was calculated to contain mainly Fe and Mn with 1.08 wt% and 0.25 wt%, respectively (Table 1C). The mass balance for Fe and Mn was confirmed, as shown by the result calculated in Table 1C. The nFeMn powder also included NaCl formed during freeze-drying of the reaction mixture, which originated from Cl in the HCl solution used in the leaching of FeMn wad and from Na in the NaOH (50% w/v) solution used for pH adjustment of FeMn acidic solution. Comparing the calculated composition of nFeMn powder (Table 1C) with that of the XRF fusion disk analysis (Table 1D), we observed a good agreement between the XRF and the calculated values. Although the XRF values were slightly lower than the calculated values, this can be attributed to the fact that some of the Fe and Mn could have been lost due to nFeMn powder containing natural organic matter from RTea; however, the overall trend from XRF agrees with the calculation. The NaCl content of nFeMn powder was 42.3%, according to the XRF analysis. The ICP-OES and IC analyses of water-leached nFeMn powder were done to cross-check the Na content and determine the Cl content. Still, the spectroscopic analysis did not produce reliable results due to the presence of natural organic matter. Due to these challenges, TG–DTA was applied and indicated that after subtracting the RTea, Fe, and Mn components from 100%, the remaining mass, NaCl in nFeMn, was approximately 92.2 wt% (Fig. S1).

Moreover, the redox potential of RTea extract was measured to be + 0.27 V by cyclic voltammetry (Fig. S2). This value is similar to other tea extracts (black and green teas + 0.23 V) and low compared to plant extracts (e.g., *T. Chebula* + 0.63 V and Eucalypus leaves + 0.4 V). The redox potentials of $Fe^{3+}$/ $Fe^{2+}$ and $Fe^{2+}$/ Fe are + 0.77 V and − 0.44 V, respectively (Mohan Kumar et al. 2013; Wang 2013). This value implies that $Fe^{3+}$ can be reduced to $Fe^{2+}$ using RTea extract. As for the reduction of $Fe^{2+}$ to Fe, there is less agreement in the literature. Some reports show the formation of nano zerovalent iron (nZVI) in the green-synthesized nano iron particles via XRD analyses using green tea extracts (Kozma et al. 2016; Zhu et al. 2018). Another report on green tea extract-synthesized nano iron particles determined no ZVI but $Fe^{3+}$ and $Fe^{2+}$ in the product via Mössbauer spectrometry (Markova et al. 2014). Another report on nano iron particles synthesized using Eucalyptus leaves indicated that $Fe^{2+}$ is difficult to reduce to ZVI because polyphenol ligands strongly stabilize $Fe^{3+}$ over $Fe^{2+}$. A complex structure was proposed in which ferric ion is located in spherical nanoparticles chelated by polyphenols (Wang 2013). The reduction potential of $Mn^{2+}$/Mn is − 1.18 V, indicating that $Mn^{2+}$ is more difficult to reduce by RTea extract than $Fe^{2+}$.

Figure 2A shows the UV–Vis spectra of FeMn acidic solution, RTea extract, and nFeMn in solution. The nFeMn in the solution was obtained by adding the pH-adjusted FeMn solution into the RTea extract. An instant color change was observed after mixing the two solutions because of the reduction of the metal ions, indicating the formation of RTea-capped nFeMn (Hoag et al. 2009). In Fig. 2A, a spectral comparison of peaks was made using the stable FeMn acidic solution instead of pH-adjusted FeMn solution, which was prone to oxidation and, therefore, immediately employed in the nFeMn synthesis reaction. The FeMn acidic solution exhibited a peak at 335 nm and the RTea extract exhibited a peak at 282 nm, belonging to the polyphenols it contained (Joubert et al. 2013). Eleven polyphenols in wine also showed peaks at 250–350 nm (Gorinstein et al. 1993). The RTea-capped nFeMn suspension exhibited no peak but a broad shoulder between 260 and 400 nm where the peaks of RTea and FeMn were placed, implying that the hump was due to a reaction between RTea polyphenols and nFeMn particles. The shifted position of the broad hump of nFeMn compared to the peak of FeMn acidic solution confirmed this reaction and the formation of polyphenol-stabilized nanoparticles.

The second set of experiments (Fig. 2B) was done to see the difference between UV–Vis spectra of FeMn acidic solution and a prepared mixture of Fe and Mn (FeMnmix)

**Table 1** Chemical analysis of the FeMn wad, FeMn acidic solution, and nFeMn powder

| (A) | Material | | Method | |
|---|---|---|---|---|
| | FeMn wad | | XRF | |
| | Bulk composition (%) | | Elemental composition (%)* | |
| | $Fe_2O_3$ | 57.5 | Fe | 40.2 |
| | MnO | 15.2 | Mn | 11.7 |
| | $Al_2O_3$ | 3.13 | Al | 1.66 |
| | $TiO_2$ | 0.16 | Ti | 0.10 |
| | $SiO_2$ | 15.6 | Si | 0.00 |
| | $K_2O$ | 0.33 | K | 0.27 |
| | MgO | 0.21 | Mg | 0.13 |
| | $Na_2O$ | 0 | Na | 0.00 |
| | LOI | 7.55 | | |
| | other | 0.23 | | |
| | Total | 99.9 | | |
| (B) | Material | | Method | |
| | FeMn acidic solution | | ICP-OES | |
| | Elemental composition (%) | | Fe recovered in the FeMn Acidic solution [yield] % | |
| | Fe | 0.34 | Fe | 84.8 |
| | Mn | 0.08 | Mn | 68.4 |
| | Al | 0.01 | Al | negligible |
| | Ti | 0.00 | Ti | 0.00 |
| | Si | 0.00 | Si | 0.00 |
| | K | 0.01 | K | negligible |
| | Mg | 0.00 | Mg | 0.00 |
| | Na | 0.00 | Na | 0.00 |
| (C) | Material | Method | (D) Material | Method |
| | nFeMn powder | calculation | nFeMn powder | XRF |
| | Elemental composition (%) ** | | Elemental composition (%) | |
| | Fe | 1.08 | Fe | 0.90 |
| | Mn | 0.25 | Mn | 0.08 |
| | | | Na | 42.3 |
| | | | LOI | 2.46 |

*Oxides in the bulk composition were converted to elemental (mg/L) and subsequently percent values

**The elemental composition of nFeMn was calculated using the ICP-OES results from (B), the volume of acid used in the synthesis, and the weighed amount of the material

from the salts of $Fe^{3+}$ and $Mn^{2+}$, the concentration of which was similar to that of FeMn acidic solution (Table 1C). In Fig. 2B, the FeMnmix showed a peak at 292 nm arising mainly from Fe(III) since Mn(II) had only a tiny peak at 200 nm. No shift was observed in the position of FeMnmix compared to the Fe(III) peak, which is indicative of no reaction occurring when mixing Fe(III) and Mn(II) solutions. On the other hand, the shifted position of the peak of the FeMn acidic solution relative to FeMnmix can be related to the particle sizes of Fe and Mn, as well as to the trace quantity of metallic impurities from the wad and chloro-complexes of Fe(III) and Mn(II) even though they were in low concentrations in the aqueous solution prepared by 50 times dilution of FeMn acidic solution for UV–vis measurement. Figure 2C shows the FTIR analysis of RTea leaves. The spectral information between 3800 and 2600 $cm^{-1}$ and 2000 and 600 $cm^{-1}$ is essential to identify the tea under investigation because all the major and minor organic constituents in teas exhibit peaks in these ranges. The FTIR spectrum of RTea leaves showed a broad peak at 3285 $cm^{-1}$ due to OH stretching vibrations. The peaks at 1615 and 1509 $cm^{-1}$ correspond to the C=C stretching of ring vibrations (Luo

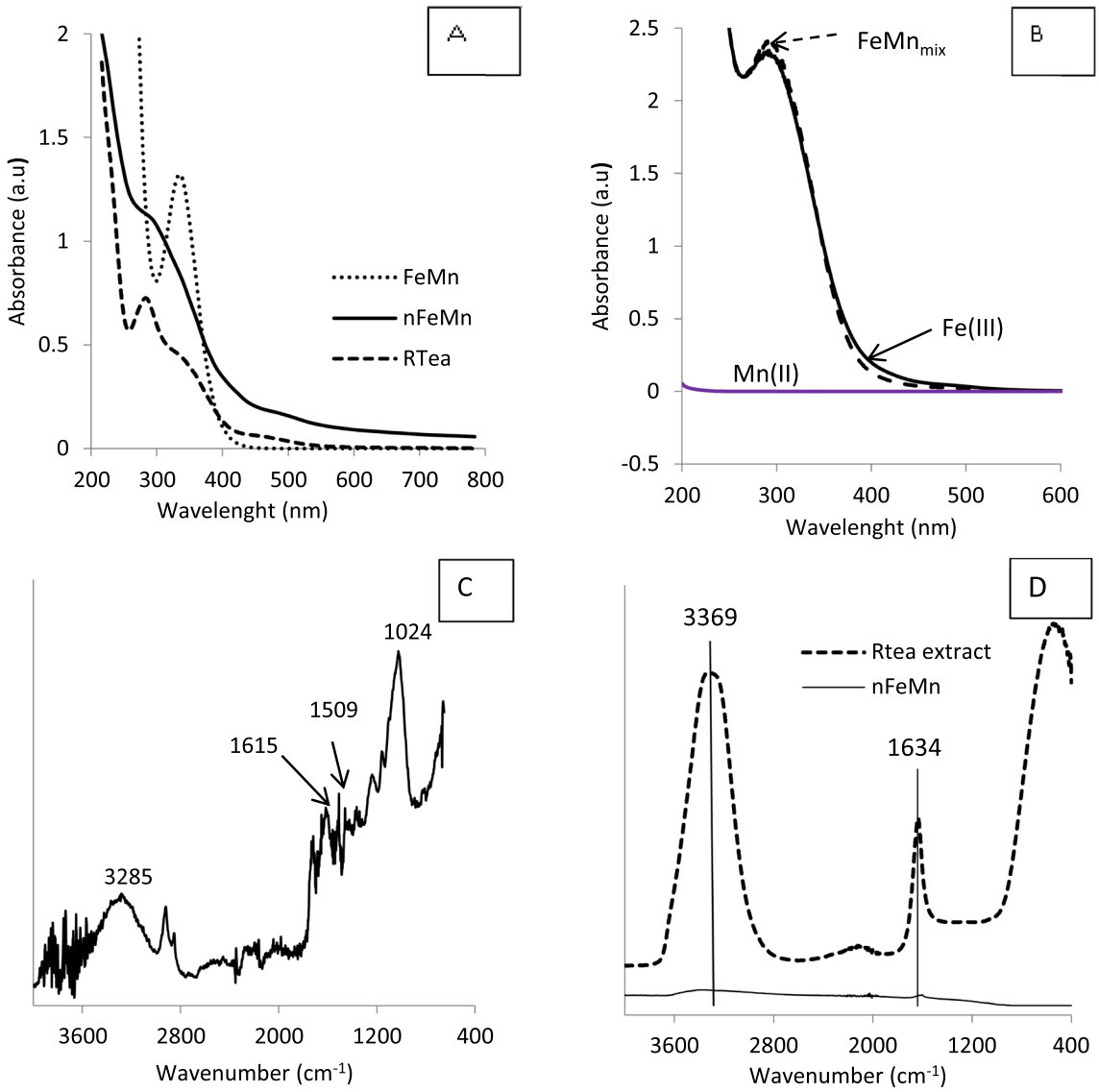


**Fig. 2** UV–Vis spectra of FeMn, nFeMn, and RTea (**A**) Mn, Fe, and Mn/Fe mixture with the same concentration as that in nFeMn (**B**) 50 times dilution. FTIR spectra of (**C**) RTea extract and nFeMn powder (**D**)

et al. 2014; Morikawa et al. 2015). The peak at 1024 cm$^{-1}$ was assigned to C–O–C and C–OH vibrations (Kora et al. 2010; Zheng and Wang 2012; Govarthanan et al. 2014). Figure 2D shows FTIR spectra of the RTea extract and the RTea-capped nFeMn powder. In the FTIR spectrum of RTea extract, the intense peak at 3369 cm$^{-1}$ is attributed to O–H stretching vibrations (Huang et al. 2015). The small peak at 1634 cm$^{-1}$ is again assigned to C=C stretching vibrations of the aromatic ring in RTea, a few of which combine to form polyphenols. It was previously demonstrated that C=C and C–O groups in the plant extracts generally have a substantial effect on the capping of nanoparticles (Kharissova et al. 2013). The RTea-capped nFeMn powder showed only a tiny peak at 1632 cm$^{-1}$, which was formed by slight shifting and extinction of the 1634 cm$^{-1}$ peak of the RTea extract, indicating that the RTea extract successfully coated nanoparticles.

TEM-EDS was used to analyze the particle size and elemental mapping of the binary nFeMn nanoparticles. The TEM images showed that the nanoparticles had well-defined borders. The TEM image recorded at high magnification showed spherical binary nFeMn particles with diameters of about 20 and 15 nm, respectively (Fig. 3A). They had a core–shell structure. They showed electron density banding where the core is darker than the less dense shell (Mallin and Murphy 2002). Figure 3B shows an image of a nFeMn particle made with the rooibos reductant. The lattice fringes on the particle indicate some degree of crystallinity in the

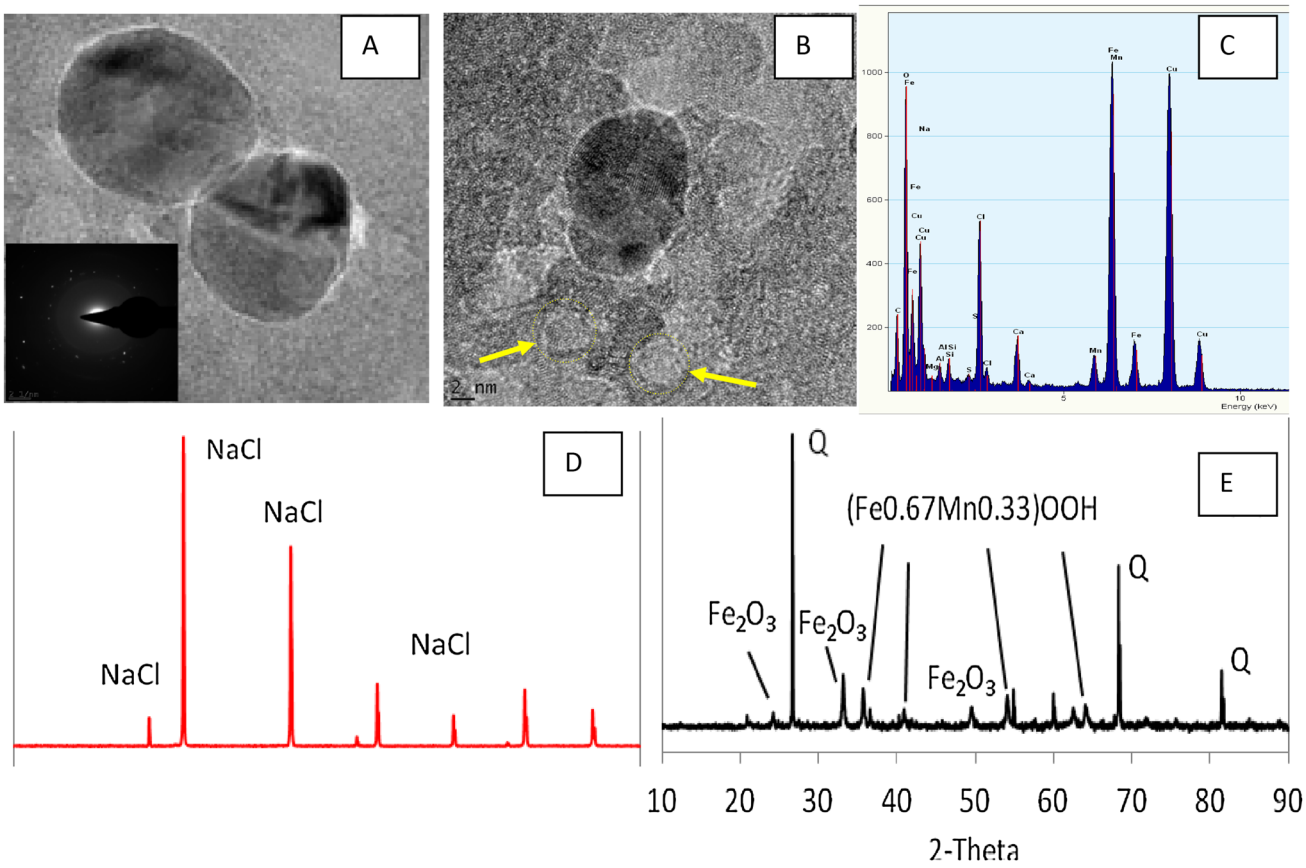


**Fig. 3** TEM images of nFeMn particles were dropped onto the TEM grid (**A–B**) EDS spectra (**C**). XRD plots of nFeMn (**D**) and FeMn wad (**E**)

material. It is possible to identify the Fe and Mn from the TEM image by measuring lattice distances on the core and shell (Liu et al. 2012). However, the d-spacing values measured on the core and shell showed some variation when compared to normal d-spacing values of Fe and Mn. The reasons may be due to the strained shell compared to the core as well as the complexity of the colloid chemistry (Strasser et al. 2010). The chemical synthesis of colloids may produce nanocrystals with a crystal structure never found in bulk materials (Sobal et al. 2002).

The selected area electron diffraction (2B) image showing electron distribution in the matrix displayed concentric circles originating from the random orientation of crystal planes [Huang polysaccharide], suggesting that the nFeMn is a polycrystalline material. The EDS analysis with ten repeats performed on the sample matrix confirmed the presence of Fe, Mn, O, Na, and Cl elements (Fig. 3D). The intense composite Fe–Mn peak dominated the matrix together with the O–Fe peak. The composite peak shows that Fe and Mn elements are in very close proximity in the sample. The Fe–O peak may indicate that polyphenols chelated Fe via their O atoms (Wang 2013).

The main peaks identified on the XRD spectrum of FeMn wad (Fig. 3D) are hematite ($Fe_2O_3$) JCPD 00-033-0664 and quartz ($SiO_2$) JCPD 01-079-1910. The existence of $(Fe_{0.67}Mn_{0.33})OOH$ JCPD 00-014-0557 is likely, but most probably due to overlapping with hematite, there is no freestanding peak of that phase. On the other hand, all the peaks clearly detected in the spectrum XRD of RTea capped nFeMn were identified to be halite (Fig. 3E). The reason that iron peaks were not observed in the XRD spectrum of nFeMn can be explained as follows: The XRD peak height depends on the size and volume fraction of nanoparticles in the nFeMn powder. XRF and ICP-OES analysis determined approximately 1% of Fe and 0.25% (w) of Mn in the nFeMn powder. Therefore, it is plausible that due to the very low metallic content, the metal peaks were below the detection limit of the XRD technique. Furthermore, the nanodomain of the particle of nFeMn does not present long-range crystallographic ordering, rendering the metal amorphous. Moreover, even if the metallic peaks were present, they would remain obscured by the well-defined halite peaks, which were the dominant phase and overlapped regions where the characteristic peaks for iron and manganese could be found.

## Application nFeMn and decoloration kinetics of MB

The effectiveness of nFeMn particles synthesized using RTea extract was probed to decolorize an aqueous solution of MB with an initial concentration of 50 mg/L, and the results are shown in Fig. 4A. The reaction between nFeMn particles and MB was instantaneous: more than 90% of MB was decolorized within 5 min of contact time. The RTea polyphenols contributed to the effectiveness of nFeMn particles due to their effectiveness in reducing and stabilizing the nanoparticles. In addition, the polyphenol-capped nanoparticles provided a large surface and contact area for MB molecules to react. The MB degradation results from this study agree with the literature using tea-polyphenols-capped nano iron particles as catalysts in Fenton-like reactions and obtaining fast degradation of dyes (Shahwan et al. 2011).

Determination of reaction kinetics is essential to understanding the decoloration mechanism of MB in the nFeMn/Fenton-like system. For this purpose, several kinetic models were applied to the experimental data (Ho et al. 2000). Among them, the pseudo-first-order kinetic model can be defined with Eq. 1 as follows:

$$\log\left(A_t - A_e\right) = \log\left(A_0 - A_e\right) - \left(\frac{k_1}{2.303}\right)t \quad (1)$$

where $A_0$ is the initial absorbance of the dye (A), $A_t$ is the absorbance of decolorized dye solution at time t, $A_e$ is the equilibrium absorbance of the dye, and $k_1$ ($min^{-1}$) is the rate constants of the pseudo-first-order kinetic equation. The graph plotted using $\log(A_t\text{-}A_e)$ versus t produced a line equation with a high correlation coefficient of $R^2 = 0.93$ (Fig. 4B). The rate constant $k_1$ was calculated from the slope and intercept of the graph. The calculated half-life value, 2.3 min, was close to the experimental results, proving that the model is correctly fitted to the data. As a result, it was concluded that the decoloration of MB followed a pseudo-first-order reaction kinetics using Eq. 2 (Bautista et al. 2007). Therefore, the pseudo-first-order kinetic rate constant ($k_1$) for the decoloration of MB was calculated to be 0.23 $A^{-1}$ $min^{-1}$.

$$-r_{MB} = k\left[C_{MB}\right][\bullet HO] \cong k'\left[C_{MB}\right] \quad (2)$$

The MB degradation could proceed through two steps: The addition of RTea-capped nFeMn into MB/$H_2O_2$ solution caused contact of RTea capping agent with MB and $H_2O_2$, resulting in some degree of decoloration of MB and initiation of radical scavenging reactions of RTea polyphenols (Joubert et al. 2005; Markova et al. 2014). Immediately after that, MB was almost entirely decolorized by the Fenton reaction, generally thought to be accompanied by some degree of mineralization. However, the degree of mineralization was not measured by Total Organic Carbon (TOC) analysis in this study (Wang et al. 2014; Yu et al. 2014). All in all, the performance of the synthesized FeMn nanoparticles is in agreement with and above the green bimetallic nanoparticles reported in the literature, as shown in Table 2.

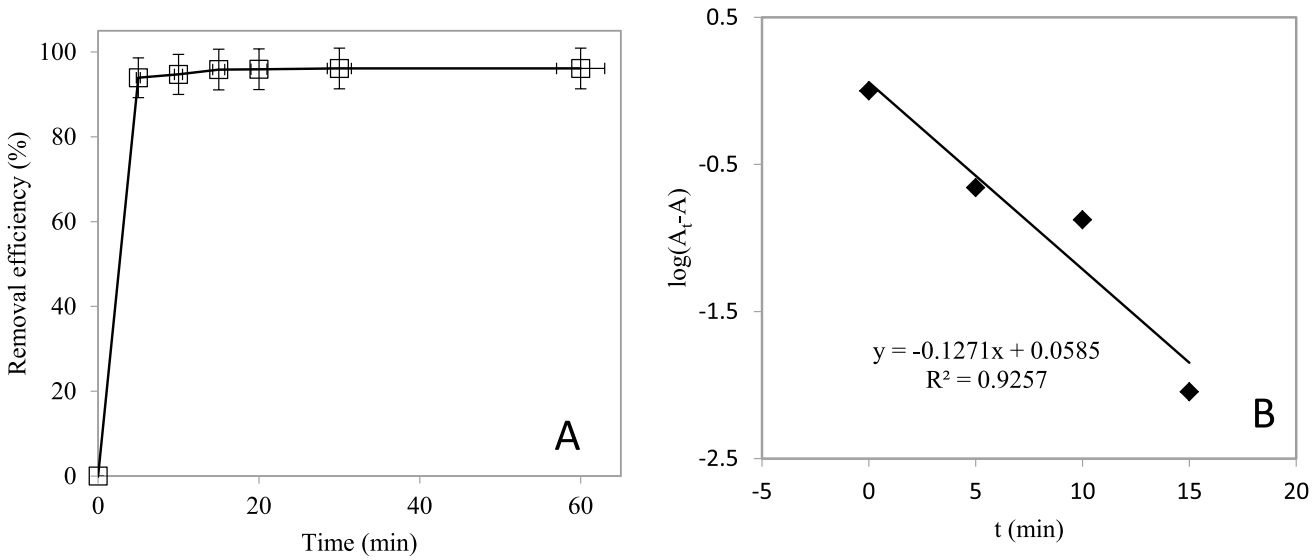


**Fig. 4** **A** Fenton-like oxidation of methylene blue using nFeMn particles capped by RTea polyphenols. Conditions: 18 mL of MB (50 mg/L), 2 mL of $H_2O_2$ (0.01%) and 0.02 g of nFeMn powder. Reaction temperature: 25 °C. **B** Linearized pseudo-first-order kinetic plots of MB

**Table 2** Summary of recent bimetallic nanoparticles synthesized from green routes

| Bimetallic catalysts | Green (plant) reducer | Application | Kinetics/performance | References |
|---|---|---|---|---|
| Fe/Pd | *Eucalyptus* leaf extract | As (III) removal from water | Pseudo-second-order model ($R^2 = 0.986$), 100% removal | Lin et al. (2021) |
| Ag–Au | Waste Tea Leaves Extract | Degradation of Congo Red and 4-Nitrophenol | 6–7 min | Kang and Kolya (2021) |
| Mn–Cu | *Vinca rosea* Extract | Degradation of Methyl red (MR), eriochrome black T (EBT), methyl orange (MO), and 4-nitrophenol | Removal efficiencies: 78.54% (MR), 87.67% (EBT), and 69.79% (MO) 1–5 min | Ahmad et al. (2022) |
| Ag–Fe | *Salvia officinalis* aqueous extract | 4-nitrophenol reduction | First-order rate, 94.56% removal efficiency, Time: 45 min | Malik et al. (2021) |
| Au–Ag | *Lawsonia inermis* seed extract | Methyl orange and 4-nitrophenol | $NaBH_4$ added, 3–18 min | Akilandaeaswari and Muthu (2021) |
| Fe/Ni | *Eucalyptus* leaf extract | Degradation of methyl orange | Pseudo first-order model, $R^2$ (> 0.89), removal efficiency 99.6% | Weng et al. (2017) |
| Ag/ZnO@Biohar | *Persicaria salicifolia* biomass | Degradation of tetracycline | Photodegradation efficiency 70.3% | Hosny et al. (2022) |
| Cu/Ag | Date palm tree leaves (*Phoenix dactylifera*) | Removal of methylene blue | The percentage removal of dye is 82.0% | Al-Haddad et al. (2020) |
| Fe/Pd | Grape leaf aqueous extract | Removal of Orange II | Removal efficiency 98% in 12 h | Luo et al. (2016) |
| FeMn | Rooibos tea extract | Methylene blue degradation | Removal efficiency 90%, 5 min | Current study |

## Conclusion

In this study, we successfully synthesized a bimetallic Rooibos Tea-capped iron and manganese nanoparticles (nFeMn) that combine iron and manganese from a ferromanganese wad mineral. The ferromanganese wad, a waste material, may be found in nature. The rooibos tea extract effectively acted as a reducing and capping agent to protect the nanoparticles. The core–shell nanoarchitecture of the synthesized nFeMn particles revealed average sizes of 15–20 nm. Because of the nFeMn powder's outstanding oxidative activity, methylene blue was degraded from solutions with concentrations ranging from 5 to 250 mg/L ppm with a removal rate of 99.99%. The performance of the prepared nFeMn was comparable with the ones reported in the literature. Given the ease of readily available raw materials used in this study (ferromanganese wad mineral and Rooibos tea), our study draws a foundation for a circular green process. Future research in this area will concentrate on three key goals: (1) A scrutinizing characterization of the nanoparticles, including DLS and Zeta potential for precise observation of particle size distribution and charge and particle stability, (2) eliminating chlorinated organics using nFeMn suspension, which has been reputed the most challenging task to date and (3) assessing the influence of varied quantities of RTea extract on reaction rate. The purpose of these assessments is to identify the most successful technique.

**Supplementary Information** The online version contains supplementary material available at https://doi.org/10.1007/s13762-023-04792-1.

**Acknowledgements** This project was partially supported by funding from NRF CSUR of South Africa.

**Authors contribution** LP, KKF: Conceptualization, Methodology, Software. NB, HO & EK: Data curation, Writing-Original draft preparation. NB & EK: Visualization, Investigation. LP, KKF: Supervision. LP, KKF, NB, HO & EK: Writing Reviewing and Editing.

**Conflict of interest** The authors declare that they have no known competing financial interests or personal relationships that could have appeared to influence the work reported in this paper.

## References

Ahmad MM, Kotb HM, Mushtaq S et al (2022) Green synthesis of Mn + Cu bimetallic nanoparticles using *Vinca rosea* extract and their antioxidant, antibacterial, and catalytic activities. Crystals. https://doi.org/10.3390/cryst12010072

Ahmed HB, Emam HE (2019) Synergistic catalysis of monometallic (Ag, Au, Pd)and bimetallic (Ag[sbnd]Au, Au[sbnd]Pd)versus trimetallic (Ag-Au-Pd)nanostructures effloresced via analogical techniques. J Mol Liq. https://doi.org/10.1016/j.molliq.2019.110975

Akilandaeaswari B, Muthu K (2021) One-pot green synthesis of Au-Ag bimetallic nanoparticles from *Lawsonia inermis* seed extract and its catalytic reduction of environmental polluted methyl orange and 4-nitrophenol. J Taiwan Inst Chem Eng 127:292–301. https://doi.org/10.1016/j.jtice.2021.07.019

Al-Haddad J, Alzaabi F, Pal P et al (2020) Green synthesis of bimetallic copper–silver nanoparticles and their application in catalytic and antibacterial activities. Clean Technol Environ Policy 22:269–277. https://doi.org/10.1007/s10098-019-01765-2

Badmus KO, Coetsee-Hugo E, Swart H, Petrik L (2018) Synthesis and characterisation of stable and efficient nano zero valent iron. Environ Sci Pollut Res 25:23667–23684. https://doi.org/10.1007/s11356-018-2119-7

Bai T, Lu P, Zhang K et al (2017) Gold/silver bimetallic nanocrystals: controllable synthesis and biomedical applications. J Biomed Nanotechnol 13:1178–1209. https://doi.org/10.1166/jbn.2017.2423

Baranska M, Schulz H, Joubert E, Manley M (2006) In situ flavonoid analysis by FT-Raman spectroscopy: identification, distribution, and quantification of aspalathin in green rooibos (*Aspalathus linearis*). Anal Chem 78:7716–7721. https://doi.org/10.1021/ac061123q

Bautista P, Mohedano AF, Gilarranz MA et al (2007) Application of Fenton oxidation to cosmetic wastewaters treatment. J Hazard Mater 143:128–134. https://doi.org/10.1016/j.jhazmat.2006.09.004

Chen Y, Liu Y, Li Y et al (2020) Synthesis, application and mechanisms of ferro-manganese binary oxide in water remediation: a review. Chem Eng J 388:124313. https://doi.org/10.1016/j.cej.2020.124313

Deng S, Zhao B, Xing Y et al (2021) Green synthesis of proanthocyanidins-functionalized Au/Ag bimetallic nanoparticles. Green Chem Lett Rev 14:43–48. https://doi.org/10.1080/17518253.2020.1861343

Doan H, Morais T, Borchtchoukova N et al (2022) Bimetallic Pt or Pd-based carbon supported nanoparticles are more stable than their monometallic counterparts for application in membraneless alkaline fuel cell anodes. Appl Catal B Environ 301:120811. https://doi.org/10.1016/j.apcatb.2021.120811

Du JT, Niu H, Wu H et al (2021) PVP-stabilized platinum nanoparticles supported on modified silica spheres as efficient catalysts for hydrogen generation from hydrolysis of ammonia borane. Int J Hydrog Energy 46:25081–25091. https://doi.org/10.1016/j.ijhydene.2021.05.062

Duan M, Jiang L, Zeng G et al (2020) Bimetallic nanoparticles/metal-organic frameworks: synthesis, applications and challenges. Appl Mater Today. https://doi.org/10.1016/j.apmt.2020.100564

Fang Z, Qiu X, Chen J, Qiu X (2011) Debromination of polybrominated diphenyl ethers by Ni/Fe bimetallic nanoparticles: influencing factors, kinetics, and mechanism. J Hazard Mater 185:958–969. https://doi.org/10.1016/j.jhazmat.2010.09.113

Fatima M, Farooq R, Lindström RW, Saeed M (2017) A review on biocatalytic decomposition of azo dyes and electrons recovery. J Mol Liq 246:275–281. https://doi.org/10.1016/j.molliq.2017.09.063

Fazlzadeh M, Rahmani K, Zarei A et al (2017) A novel green synthesis of zero valent iron nanoparticles (NZVI) using three plant extracts and their efficient application for removal of Cr(VI) from aqueous solutions. Adv Powder Technol 28:122–130. https://doi.org/10.1016/j.apt.2016.09.003

Ghohestani E, Samari F, Yousefinejad S (2022) An efficient removal of methylene blue and lead(II) from aqueous solutions by green synthesized iron oxide/pillared bentonite nanocomposite. Mater Chem Phys 287:126266. https://doi.org/10.1016/j.matchemphys.2022.126266

Gilroy KD, Ruditskiy A, Peng HC et al (2016) Bimetallic nanocrystals: syntheses, properties, and applications. Chem Rev 116:10414–10472. https://doi.org/10.1021/acs.chemrev.6b00211

Gorinstein S, Weisz M, Zemser M et al (1993) Spectroscopic analysis of polyphenols in white wines. J Ferment Bioeng 75:115–120. https://doi.org/10.1016/0922-338X(93)90221-S

Govarthanan M, Selvankumar T, Manoharan K et al (2014) Biosynthesis and characterization of silver nanoparticles using Panchakavya, an Indian traditional farming formulating agent. Int J Nanomed 9:1593–1599. https://doi.org/10.2147/IJN.S58932

Ho YS, Mckay G, Hong T et al (2000) Separation & purification reviews kinetics of pollutant sorption by biosorbents : review. Sep Purif Rev 29:189–232

Hoag GE, Collins JB, Holcomb JL et al (2009) Degradation of bromothymol blue by "greener" nano-scale zerovalent iron synthesized using tea polyphenols. J Mater Chem 19:8671–8677. https://doi.org/10.1039/b909148c

Hosny M, Fawzy M, Eltaweil AS (2022) Green synthesis of bimetallic Ag/ZnO@Biohar nanocomposite for photocatalytic degradation of tetracycline, antibacterial and antioxidant activities. Sci Rep 12:1–17. https://doi.org/10.1038/s41598-022-11014-0

Huang L, Luo F, Chen Z et al (2015) Green synthesized conditions impacting on the reactivity of Fe NPs for the degradation of malachite green. Spectrochim Acta Part A Mol Biomol Spectrosc 137:154–159. https://doi.org/10.1016/j.saa.2014.08.116

Iswaldi I, Arráez-Román D, Rodríguez-Medina I et al (2011) Identification of phenolic compounds in aqueous and ethanolic rooibos extracts (*Aspalathus linearis*) by HPLC-ESI-MS (TOF/IT). Anal Bioanal Chem 400:3643–3654. https://doi.org/10.1007/s00216-011-4998-z

Jin X, Liu Y, Tan J et al (2018) Removal of Cr(VI) from aqueous solutions via reduction and absorption by green synthesized iron nanoparticles. J Clean Prod 176:929–936. https://doi.org/10.1016/j.jclepro.2017.12.026

Joubert E, De Beer D, Malherbe CJ et al (2013) Occurrence and sensory perception of Z-2-(β-d-glucopyranosyloxy)-3- phenylpropenoic acid in rooibos (*Aspalathus linearis*). Food Chem 136:1078–1085. https://doi.org/10.1016/j.foodchem.2012.09.014

Joubert E, Winterton P, Britz TJ, Gelderblom WCA (2005) Antioxidant and pro-oxidant activities of aqueous extracts and crude polyphenolic fractions of rooibos (*Aspalathus linearis*). J Agric Food Chem 53:10260–10267. https://doi.org/10.1021/jf051355a

Kang CW, Kolya H (2021) Green synthesis of ag-au bimetallic nanocomposites using waste tea leaves extract for degradation congo red and 4-nitrophenol. Sustain. https://doi.org/10.3390/su13063318

Kharissova OV, Dias HVR, Kharisov BI et al (2013) The greener synthesis of nanoparticles. Trends Biotechnol 31:240–248. https://doi.org/10.1016/j.tibtech.2013.01.003

Kimpiab E, Kapiamba KF, Folifac L et al (2022) Synthesis of stabilized iron nanoparticles from acid mine drainage and Rooibos Tea for application as a Fenton-like catalyst. ACS Omega. https://doi.org/10.1021/acsomega.2c01846

Kora AJ, Sashidhar RB, Arunachalam J (2010) Gum kondagogu (*Cochlospermum gossypium*): a template for the green synthesis and stabilization of silver nanoparticles with antibacterial application. Carbohydr Polym 82:670–679. https://doi.org/10.1016/j.carbpol.2010.05.034

Kozma G, Rónavári A, Kónya Z, Kukovecz Á (2016) Environmentally benign synthesis methods of zero-valent iron nanoparticles. ACS Sustain Chem Eng 4:291–297. https://doi.org/10.1021/acssuschemeng.5b01185

Lin Y, Cao Y, Yao Q, Xie J (2022) Revealing the composition-dependent structural evolution fundamentals of bimetallic nanoparticles through an inter-particle alloying reaction. Chem Sci. https://doi.org/10.1039/d1sc06296d

Lin Y, Jin X, Khan NI et al (2021) Efficient removal of As (III) by calcined green synthesized bimetallic Fe/Pd nanoparticles based on adsorption and oxidation. J Clean Prod 286:124987. https://doi.org/10.1016/j.jclepro.2020.124987

Liu X, Wang D, Li Y (2012) Synthesis and catalytic properties of bimetallic nanomaterials with various architectures. Nano Today 7:448–466. https://doi.org/10.1016/j.nantod.2012.08.003

Loza K, Heggen M, Epple M (2020) Synthesis, structure, properties, and applications of bimetallic nanoparticles of noble metals. Adv Funct Mater. https://doi.org/10.1002/adfm.201909260

Luo F, Chen Z, Megharaj M, Naidu R (2014) Biomolecules in grape leaf extract involved in one-step synthesis of iron-based nanoparticles. RSC Adv 4:53467–53474. https://doi.org/10.1039/c4ra08808e

Luo F, Yang D, Chen Z et al (2016) One-step green synthesis of bimetallic Fe/Pd nanoparticles used to degrade Orange II. J Hazard Mater 303:145–153. https://doi.org/10.1016/j.jhazmat.2015.10.034

Malik MA, Alshehri AA, Patel R (2021) Facile one-pot green synthesis of Ag-Fe bimetallic nanoparticles and their catalytic capability for 4-nitrophenol reduction. J Mater Res Technol 12:455–470. https://doi.org/10.1016/j.jmrt.2021.02.063

Mallin MP, Murphy CJ (2002) Solution-phase synthesis of sub-10 nm Au − Ag alloy nanoparticles. Nano Lett 2(11):1235–1237. https://doi.org/10.1021/nl025774n

Markova Z, Novak P, Kaslik J et al (2014) Iron(II, III)-polyphenol complex nanoparticles derived from green tea with remarkable ecotoxicological impact. ACS Sustain Chem Eng 2:1674–1680. https://doi.org/10.1021/sc5001435

Mohan Kumar K, Mandal BK, Siva Kumar K et al (2013) Biobased green method to synthesise palladium and iron nanoparticles using *Terminalia chebula* aqueous extract. Spectrochim Acta Part A Mol Biomol Spectrosc 102:128–133. https://doi.org/10.1016/j.saa.2012.10.015

Mondal S, Roy N, Laskar RA et al (2011) Biogenic synthesis of Ag, Au and bimetallic Au/Ag alloy nanoparticles using aqueous extract of mahogany (*Swietenia mahogani* JACQ.) leaves. Colloids Surf B Biointerfaces 82:497–504. https://doi.org/10.1016/j.colsurfb.2010.10.007

Morikawa T, Ninomiya K, Akaki J et al (2015) Dipeptidyl peptidase-IV inhibitory activity of dimeric dihydrochalcone glycosides from flowers of *Helichrysum arenarium*. J Nat Med 69:494–506. https://doi.org/10.1007/s11418-015-0914-8

Mukherjee R, Kumar R, Sinha A et al (2016) A review on synthesis, characterization, and applications of nano zero valent iron (nZVI) for environmental remediation. Crit Rev Environ Sci Technol 46:443–466. https://doi.org/10.1080/10643389.2015.1103832

Nasrollahzadeh M, Sajjadi M, Iravani S, Varma RS (2021) Green-synthesized nanocatalysts and nanomaterials for water treatment: current challenges and future perspectives. J Hazard Mater 401:123401. https://doi.org/10.1016/j.jhazmat.2020.123401

Paquin F, Rivnay J, Salleo A et al (2015) Multi-phase semicrystalline microstructures drive exciton dissociation in neat plastic semiconductors. J Mater Chem C 3:10715–10722. https://doi.org/10.1039/b000000x

Rai HS, Bhattacharyya MS, Singh J et al (2005) Removal of dyes from the effluent of textile and dyestuff manufacturing industry: a review of emerging techniques with reference to biological treatment. Crit Rev Environ Sci Technol 35:219–238. https://doi.org/10.1080/10643380590917932

Ramos RMCR, Regulacio MD (2021) Controllable synthesis of bimetallic nanostructures using biogenic reagents: a green perspective. ACS Omega 6:7212–7228. https://doi.org/10.1021/acsomega.1c00692

Shahwan T, Abu Sirriah S, Nairat M et al (2011) Green synthesis of iron nanoparticles and their application as a Fenton-like catalyst for the degradation of aqueous cationic and anionic dyes. Chem Eng J 172:258–266. https://doi.org/10.1016/j.cej.2011.05.103

Shankar SS, Rai A, Ahmad A, Sastry M (2004) Rapid synthesis of Au, Ag, and bimetallic Au core-Ag shell nanoparticles using neem (*Azadirachta indica*) leaf broth. J Colloid Interface Sci 275:496–502. https://doi.org/10.1016/j.jcis.2004.03.003

Sheny DS, Mathew J, Philip D (2011) Phytosynthesis of Au, Ag and Au-Ag bimetallic nanoparticles using aqueous extract and dried leaf of *Anacardium occidentale*. Spectrochim Acta Part A Mol Biomol Spectrosc 79:254–262. https://doi.org/10.1016/j.saa.2011.02.051

Sivashankar R, Thirunavukkarasu A, Nithya R et al (2022) Karanja oil transesterification using green synthesized bimetallic oxide catalyst, gCaO-$CeO_2$: comparative investigations with the monometallic oxide catalysts on the catalytic efficacy and stability. Fuel 319:123711. https://doi.org/10.1016/j.fuel.2022.123711

Smuleac V, Varma R, Sikdar S, Bhattacharyya D (2011) Green synthesis of Fe and Fe/Pd bimetallic nanoparticles in membranes for reductive degradation of chlorinated organics. J Membr Sci 379:131–137. https://doi.org/10.1016/j.memsci.2011.05.054

Sobal NS, Hilgendorff M, Mŏhwald H et al (2002) Synthesis and structure of colloidal bimetallic nanocrystals: the non-alloying system Ag/Co. Nano Lett 2:621–624. https://doi.org/10.1021/nl025533f

Stefaniuk M, Oleszczuk P, Ok YS (2016) Review on nano zerovalent iron (nZVI): from synthesis to environmental applications. Chem Eng J 287:618–632. https://doi.org/10.1016/j.cej.2015.11.046

Strasser P, Koh S, Anniyev T et al (2010) Lattice-strain control of the activity in dealloyed core-shell fuel cell catalysts. Nat Chem 2:454–460. https://doi.org/10.1038/nchem.623

Suliz KV, Kolosov AY, Myasnichenko VS et al (2022) Control of cluster coalescence during formation of bimetallic nanoparticles and nanoalloys obtained via electric explosion of two wires. Adv Powder Technol 33:103518. https://doi.org/10.1016/j.apt.2022.103518

Tiri RNE, Gulbagca F, Aygun A et al (2022) Biosynthesis of Ag–Pt bimetallic nanoparticles using propolis extract: antibacterial effects and catalytic activity on $NaBH_4$ hydrolysis. Environ Res 206:112622. https://doi.org/10.1016/j.envres.2021.112622

Toshima N, Yonezawa T (1998) Bimetallic nanoparticles - novel materials for chemical and physical applications. New J Chem 22:1179–1201. https://doi.org/10.1039/a805753b

Wang Q, Tian S, Ning P (2014) Degradation mechanism of methylene blue in a heterogeneous fenton-like reaction catalyzed by ferrocene. Ind Eng Chem Res 53:643–649. https://doi.org/10.1021/ie403402q

Wang Z (2013) Iron complex nanoparticles synthesized by eucalyptus leaves. ACS Sustain Chem Eng 1:1551–1554. https://doi.org/10.1021/sc400174a

Weng X, Guo M, Luo F, Chen Z (2017) One-step green synthesis of bimetallic Fe/Ni nanoparticles by eucalyptus leaf extract: biomolecules identification, characterization and catalytic activity. Chem Eng J 308:904–911. https://doi.org/10.1016/j.cej.2016.09.134

Yang M, Somorjai GA (2004) Unusual hydrogen effect in olefin dehydrogenation: 1-methylcyclohexene dehydrogenation initiated by excess hydrogen over Pt(1 1 1) surfaces, a combined sum frequency generation spectroscopy and kinetic study. J Phys Chem B 108:4405–4410. https://doi.org/10.1021/jp036835o

Yoo CJ, Dong WJ, Park JY et al (2020) Compositional and geometrical effects of bimetallic Cu-Sn catalysts on selective electrochemical $CO_2$ reduction to CO. ACS Appl Energy Mater 3:4466–4473. https://doi.org/10.1021/acsaem.0c00157

Yu C, Li G, Wei L et al (2014) Fabrication, characterization of β-$MnO_2$ microrod catalysts and their performance in rapid degradation of dyes of high concentration. Catal Today 224:154–162. https://doi.org/10.1016/j.cattod.2013.11.029

Zhan G, Huang J, Du M et al (2011) Green synthesis of Au-Pd bimetallic nanoparticles: single-step bioreduction method with plant

extract. Mater Lett 65:2989–2991. https://doi.org/10.1016/j.matlet.2011.06.079

Zhang X, Yan R, Zhou W, Zhou S (2022) Pt–Ru bimetallic nanoparticles anchored on carbon nanotubes/polyaniline composites with coral-like structure for enhanced methanol oxidation. J Alloy Compd 920:165990. https://doi.org/10.1016/j.jallcom.2022.165990

Zhang Y, Wang J, Su Z et al (2020) Spinel $MnFe_2O_4$ nanoparticles (MFO-NPs) for $CO_2$ cyclic decomposition prepared from ferromanganese ores. Ceram Int 46:14206–14216. https://doi.org/10.1016/j.ceramint.2020.02.229

Zheng Y, Wang A (2012) Ag nanoparticle-entrapped hydrogel as promising material for catalytic reduction of organic dyes. J Mater Chem 22:16552–16559. https://doi.org/10.1039/c2jm32774k

Zhu F, Ma S, Liu T, Deng X (2018) Green synthesis of nano zerovalent iron/Cu by green tea to remove hexavalent chromium from groundwater. J Clean Prod 174:184–190. https://doi.org/10.1016/j.jclepro.2017.10.302